System-Level Energy Characterization of an Automotive PEM Fuel Cell Model Using Quasi-Steady Extraction and Local Sensitivity

Emil D. Maer
Electrical Machines and Drives Dept.
Technical University of Cluj-Napoca
Cluj-Napoca, Romania
emil.maer@emd.utcluj.ro

Daniel Fodorean
Electrical Machines and Drives Dept.
Technical University of Cluj-Napoca
Cluj-Napoca, Romania
daniel.fodorean@emd.utcluj.ro

Mircea Răceanu
ICSI Energy, National Research and Development Institute for Cryogenic and Isotopic Technologies
240050 Râmnicu Vâlcea , Romania
mircea.raceanu@icsi.ro

Elena Carcadea
ICSI Energy, National Research and Development Institute for Cryogenic and Isotopic Technologies
240050 Râmnicu Vâlcea , Romania
elena.carcadea@icsi.ro

***Abstract*—This paper analyzes an automotive proton exchange membrane fuel cell (PEMFC) system model using unified energy metrics on hydrogen lower heating value. We extract quasi-steady operating points from a stepped power profile and compute polarization and power characteristics together with net system performance, including compressor and pump power. We define hydrogen utilization from window integrals of fresh inlet and consumed hydrogen mass flow and we investigate transient effects. We quantify normalized local sensitivities at three load levels using ±10% central perturbations for key electrochemical and operating parameters. Finally, we verify the consistency of system-level trends on a custom 2500 s (more than 41 minutes) dynamic power-demand profile and report integrated energy and fuel consumption indicators. The results rank the most influential parameters on voltage, net power, and hydrogen consumption and provide practical guidance for robust model-based system studies.**

Keywords—PEM fuel cell, system modeling, LHV efficiency, stepped load, local sensitivity, dynamic power-demand.

I. INTRODUCTION

Proton exchange membrane fuel cells (PEMFC) support electrified propulsion due to high specific energy of hydrogen and scalable stack power [1]. System level performance depends on electrochemical losses, reactant management, humidification, thermal control, and auxiliary power [2], [3]. A consistent evaluation requires metrics that connect electrical output, hydrogen consumption, and balance of plant power [4]. In this work we use a detailed system model implemented in *MATLAB/Simulink* and *Simscape*, based on a reference architecture from MathWorks [5]. We focus on two complementary regimes. We first construct quasi-steady operating points from a stepped power profile to obtain a clean polarization map and derived energy metrics. We then quantify normalized local sensitivities at representative load levels to rank the influence of key parameters on voltage, net power, and hydrogen consumption. Finally, we verify the system-level trends on a custom 2500 s dynamic power-demand profile that excites auxiliaries and thermal behavior. The main contribution of this paper consists in the reproducible workflow that links quasi-steady mapping, sensitivity ranking, and dynamic-profile consistency checks under the same model assumptions. The simulated PEMFC system architecture is summarized in Section II.

This work was supported by a grant co-financed by the European Regional Development Fund, within the Smart Growth, Digitization and Financial Instruments Program 2021-2027, as part of project Romanian Hub for Hydrogen and new energy technologies-Ro-HydroHub, contract no G 2025-113330 din 30.09.2025 to G 2024-81692/390006 from 13.11.2024, SMIS code: 351358.

II. MODEL AND EVALUATION METHODOLOGY

A. PEMFC system model

We use a proton exchange membrane fuel cell system model that includes a compressed air supply subsystem, anode and cathode humidification, anode and cathode gas channels, a stack membrane electrode assembly (MEA) block, and a thermal management loop with pump and radiator. In this paper, MEA denotes the electrochemical stack sub-model that computes cell voltage and reaction-related mass and heat flows from local operating conditions.

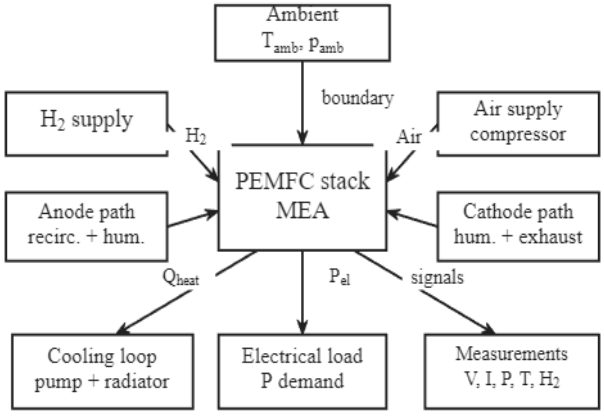

Fig. 1. Simplified system architecture of the simulated PEM fuel cell model.

The model includes auxiliary electric loads such as the air compressor drive and coolant pump. We log stack electrical variables, reactant mass flows, pressures, and auxiliary powers at system interfaces [5]. For quasi-steady mapping we apply a stepped power profile. Each step uses a ramp segment and a hold segment. We define the end time of step k as

$t_{\mathrm{end},k}$ and we compute averages on a fixed window [t1, t2] placed at the end of the hold. We use:

$$T_{\mathrm{avg}} = t_2 - t_1 = 10\,\mathrm{s} \tag{1}$$

This window reduces transient influence and provides stable operating points [6], [7]. For dynamic verification, we use a custom 2500 s power-demand profile, defined by the variables drive_cycle_time and drive_cycle_power and imposed on the electrical load subsystem in kW. The profile is not a standard named vehicle cycle, but a dynamic load profile with repeated low-, medium-, and high-power excursions. It is used to excite stack power, auxiliary power, and thermal states under time-dependent operating conditions. We report integrated energy and fuel consumption indicators over the full cycle [8], [9].

The six operating points were selected to cover the usable load range of the simulated PEMFC system, from low-load operation to near-rated stack power. The corresponding stack power levels range from 20 kW to 110 kW, which allows the comparison of voltage, efficiency, reactant demand, auxiliary power, and hydrogen utilization across representative operating conditions.

B. Energy metrics and quasi-steady extraction

First, we use hydrogen lower heating value LHV_{H_2} = 33.33 kWh/kg as the reference chemical energy [4], [9], [10]. We compute electrical energy as the time integral of stack electrical power [11].

Next, we define the electrical energy produced over an interval [t1, t2] as:

$$E_{el} = \int_{t_1}^{t_2} P_{stack}(t)\ dt \tag{2}$$

The hydrogen mass consumed over the same interval is:

$$m_{H_2,cons} = \int_{t_1}^{t_2} \dot{m}_{H_2,cons}(t)\ dt \tag{3}$$

The fresh inlet hydrogen mass is:

$$m_{H_2,\mathrm{in}} = \int_{t_1}^{t_2} \dot{m}_{H_2,\mathrm{in}}(t)\ dt \tag{4}$$

The hydrogen utilization on the interval is defined as:

$$U_{H_2} = \frac{m_{H_2,\mathrm{cons}}}{m_{H_2,\mathrm{in}}} \tag{5}$$

LHV electrical efficiency on the interval is:

$$\eta_{\mathrm{LHV}} = \frac{E_{\mathrm{el}}}{m_{H_2,\mathrm{in}} \cdot LHV_{H_2}} \tag{6}$$

Specific useful energy is defined as:

$$E_{\mathrm{spec}} = \frac{E_{\mathrm{el}}}{m_{H_2,\mathrm{in}}} \tag{7}$$

We define the net electrical power as being the stack power minus the auxiliary power [12].

$$P_{\mathrm{net}}(t) = P_{\mathrm{stack}}(t) - P_{\mathrm{aux}}(t), \tag{8}$$

where $P_{\mathrm{aux}}(t)$ includes compressor and pump power when active.

We report window averages for quasi-steady points and cycle integrals for the dynamic profile. The hydrogen utilization factor is treated as a window-based apparent utilization value, not as an instantaneous single-pass utilization value. Its detailed interpretation is discussed together with the results.

C. Compressor speed reconstruction

For each step k, the analysis window $[t_1, t_2]$ is defined as the last $T_{\mathrm{avg}} = 10\,\mathrm{s}$ of the hold period. The average values reported in the tables are computed as simple time averages over this window:

$$\overline{y_k} = \frac{1}{t_2 - t_1}\int_{t_1}^{t_2} y(t)\ dt \tag{9}$$

The compressor is the main consumer at PEMFC system level [13]. The compressor shaft speed is not directly available in the model as an angular speed signal. However, the model provides the signal *comp_rpm*as a normalized command in the range 0 to 1. The compressor speed axis *comp_rpm_TLU* from the *Model Workspace* is used to determine the maximum speed, $rpm_{\max}$. The equivalent instantaneous speed is then obtained as:

$$rpm(t) = u_{cmd}(t) \cdot rpm_{max}$$
$$rpm_{max} = max(comp_rpm_TLU). \tag{10}$$

The stepwise mean compressor speed is:

$$rpm_{comp,k} = \frac{1}{t_2 - t_1}\int_{t_1}^{t_2} rpm\,(t)\ dt \tag{11}$$

This definition yields a signal compatible with the compressor map and enables direct correlation with compressor output power P_{comp} and the supply pressures. This reconstruction enables consistent interpretation of compressor power and cathode supply behavior across operating points.

D. Local sensitivity method

We quantify local sensitivities at three load levels j_{low}, j_{mid}, and j_{high}. For each parameter θ we apply a ±10% perturbation around the nominal value and compute the central finite difference sensitivity on an output y.

The normalized local sensitivity is defined as:

$$S_{y,\theta} = \left(\frac{\theta_0}{y_0}\right) \cdot \frac{y(1.10 \cdot \theta_0) - y(0.90 \cdot \theta_0)}{0.20 \cdot \theta_0} \tag{12}$$

Here, θ0 is the nominal parameter value and y0 is the baseline output obtained at θ0.

Sensitivities are reported for three outputs: V_{cell} for voltage performance, P_{net} for system usable power, and $\dot{m}_{H_2,\mathrm{cons}}$ or m_{H_2} over the window for fuel usage [14]. We evaluate each sensitivity at the quasi-steady windows extracted from the stepped profile. The parameter set includes the relevant MEA electrochemical parameters and operating parameters with direct impact, such as pressure or humidity offsets [6]. In this work, $m_{H_2,\mathrm{cons}}$ over each quasi-steady window are primarily constrained by Faraday's law at fixed current demand. Since the current density is imposed by the stepped profile in each window, perturbations of electrochemical and operating parameters change V_{cell} and auxiliary power but have a negligible effect on the consumed hydrogen mass. Therefore, S_H2 is expected to be

approximately zero for the considered parameter set and operating points.

The study is limited to model-based system characterization. The analysis does not include experimental stack validation, detailed degradation mechanisms, purge strategy optimization, or full compressor map calibration. Therefore, the results should be interpreted as a reproducible simulation-based assessment of system trends, rather than as a final validated performance prediction for a specific commercial PEMFC unit.

III. RESULTS AND DISCUSSION

A. Quasi-steady step mapping

The extended polarization table reports, for each step, the current density, voltages, stack power, consumed and fresh hydrogen flow rates, pressures, compressor speed, and auxiliary power. All quantities are computed as averages over the 10 s window at the end of the hold period. This table provides a direct and coherent description of the operating regimes. Minor non-monotonic variations in P_{pump} across steps can occur because pump demand is set by the cooling control states and thermal transients, not by P_{stack} alone, and all values are reported as 10 s end-window averages. To improve readability, the extended polarization dataset is split into:

(i) main electrical variables and performance metrics (Table I).

(ii) gas-side boundary conditions and auxiliary variables (Table II).

Figure 2 shows the polarization curve obtained from quasi-steady points. The curve highlights the voltage decrease with increasing current density, and its shape is consistent with the standard interpretation in terms of activation, ohmic, and mass-transport losses.

Figure 3 highlights the difference between stack-level performance and system-level performance. At high current densities, the increased air demand drives up P_{comp}, and P_{net} is reduced relative to P_{stack}. This result is critical for system sizing and control strategies, because the useful power available for propulsion is constrained by auxiliary consumption.

TABLE I. EXTENDED POLARIZATION TABLE, ELECTRICAL METRICS

step	t_1 s	t_2 s	j A/cm^2	I_{stack} A	V_{cell} V	V_{stack} V	P_{stack} kW	η_{LHV}	P_{net} kW
1	25	35	0.17152	48.025	1.0411	416.45	20	0.83051	19.33
2	60	70	0.36094	101.06	0.98949	395.79	40	0.78955	38.583
3	95	105	0.59697	167.15	0.89757	359.03	60	0.72617	57.702
4	130	140	0.84202	235.77	0.84831	339.32	80	0.67678	76.645
5	165	175	1.0564	295.79	0.8452	338.08	100	0.67424	95.778
6	200	210	1.1656	326.35	0.84264	337.06	110	0.67217	105.33

TABLE II. EXTENDED GAS-SIDE AND AUXILIARY VARIABLES FOR QUASI-STEADY STEP POINTS

step	t_1 s	t_2 s	$\dot{mH}_2$ [kg/s]	$mH_{2,\text{in}}$ [kg/s]	$\dot{mO}_2$ [kg/s]	$p_{\text{an,in}}$ bar	$p_{\text{ca,in}}$ bar	rpm_{comp}	P_{comp} kW	P_{pump} kW	U_{H_2} pu
1	25	35	0.00020068	0.00018787	0.0015927	1.6123	1.6161	368.22	0.66977	0	1.0683
2	60	70	0.0004223	0.00039779	0.0033517	1.6092	1.62	783.01	1.4168	0	1.0607
3	95	105	0.00069846	0.00067609	0.0055435	1.6033	1.6254	1280.6	2.298	8.6135e-05	1.0268
4	130	140	0.00098518	0.00098988	0.007819	1.594	1.6318	1885.5	3.345	0.0095474	0.99515
5	165	175	0.001236	0.0012417	0.0098096	1.5843	1.6375	2402.6	4.2148	0.0075532	0.99543
6	200	210	0.0013637	0.0013697	0.010823	1.5788	1.6406	2672.4	4.6586	0.0075028	0.99566

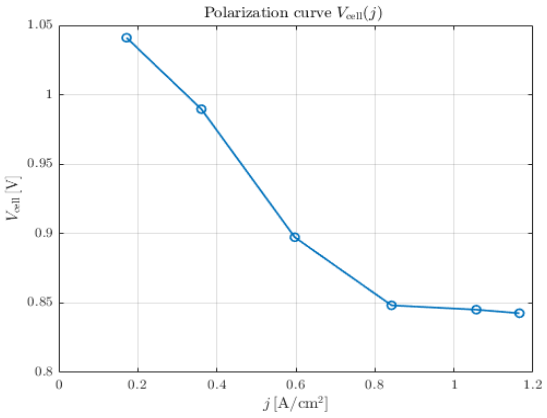

Fig. 2. Polarization curve $V_{\text{cell}}(j)$ from quasi-steady step points, computed as 10 s end of hold averages.

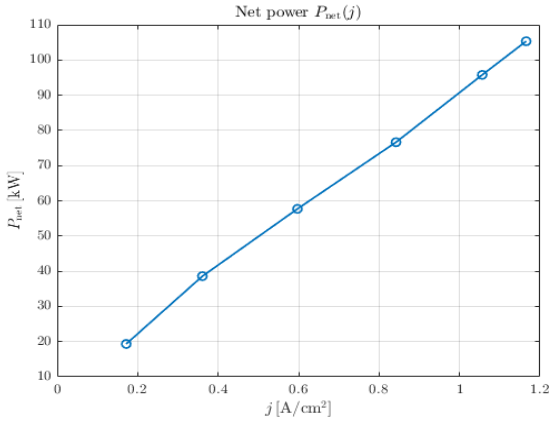

Fig. 3. Net system power $P_{\text{net}}(j)$ from quasi-steady step points, including auxiliary consumption.

Figure 4 shows the evolution of electrical efficiency, referenced to the LHV. Efficiency decreases as current density increases, because voltage decreases and reactant consumption increases. At high-load conditions, an increasing share of the chemical energy is converted into heat and auxiliary loads, which reduces overall efficiency.

Figure 5 reports hydrogen utilization computed as the ratio between window-integrated consumed hydrogen mass flow and fresh inlet hydrogen mass flow. At medium and high loads, utilization remains below unity and stable.

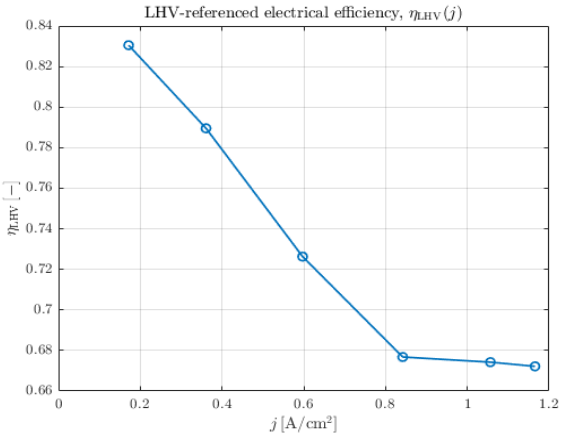

Fig. 4. LHV referenced efficiency $\eta_{\text{LHV}}(j)$ from quasi-steady step points.

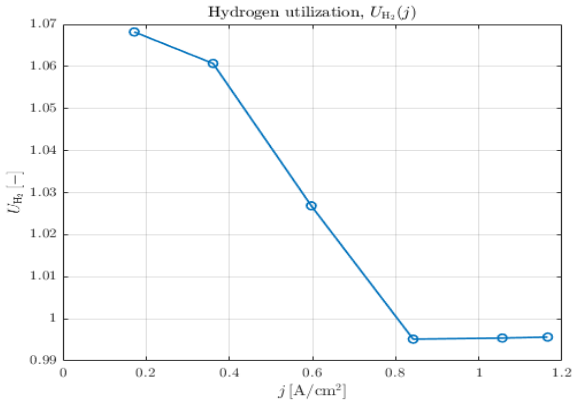

Fig. 5. Hydrogen utilization $U_{\text{H}_2}(j)$ from quasi-steady step points, computed over the 10 s end of hold window.

At low loads, U_H2 values slightly above unity can occur because the reported values are computed over finite 10 s averaging windows as the ratio between consumed hydrogen and fresh inlet hydrogen. Therefore, they represent apparent window-based utilization, not instantaneous single-pass utilization. In the first low-load windows, the anode recirculation loop and internal gas volumes can temporarily supply hydrogen already stored in the system. Since the current model does not have a direct stored-hydrogen inventory signal, a fully corrected inventory balance would require additional volume and composition assumptions. For this reason, U_H2 is used here as a consistent comparative metric over identical quasi-steady windows.

The PEMFC input and output trends are summarized in Fig. 6. Because the plotted quantities have different physical units, each signal is divided by its own maximum value and shown as a relative value. Panel (a) shows the gas-side and auxiliary variables, while panel (b) shows the electrical output and performance variables. Reactant supply and compressor demand increase with current density, while cell voltage and LHV efficiency decrease as load increases.

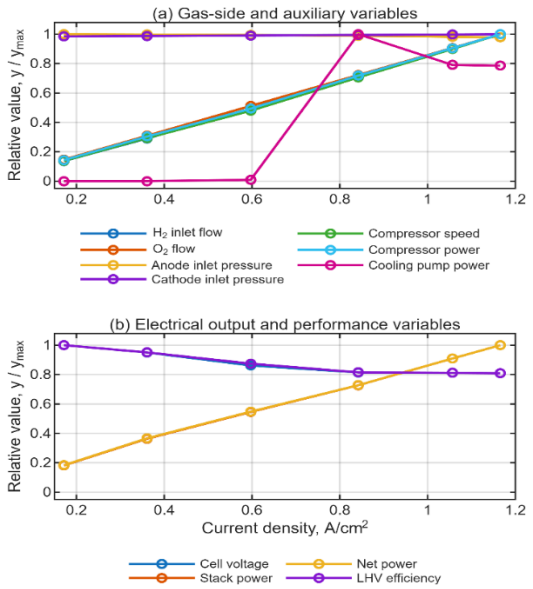

Fig. 6. Relative quasi-steady PEMFC input and output trends as a function of current density. Each variable is normalized to its own maximum value to allow comparison between quantities with different physical units.

The cooling pump does not follow stack power monotonically because it is driven by the thermal management loop, not directly by electrical load. The 10 s averaging windows may capture transient cooling states after load ramps, so small variations in pump power should be interpreted as control response effects rather than fully stabilized steady-state thermal demand.

B. *Local sensitivity at three load levels*

Table III reports normalized local sensitivities at three operating points. Positive values indicate that the output increases with the tested parameter, while negative values indicate the opposite trend. Large absolute values identify parameters that require careful calibration because they strongly affect cell voltage and net power. Hydrogen-related sensitivities remain small in this study because the current density is imposed by the load profile.

TABLE III. NORMALIZED LOCAL SENSITIVITIES (±10% CENTRAL DIFFERENCE) OF CELL VOLTAGE AND NET POWER AT THREE OPERATING POINTS.

j A $/cm^2$	Parameter	S_V (V_{cell})	S_P (P_{net})	S_H2 ($m_{H_2,}$)
0.4	stack_io	0.018854	0.01911	0.0000
0.4	stack_alpha	0.16154	0.16175	0.0000
0.4	stack_t_membrane	-0.075927	-0.076042	0.0000
0.4	env_RH	0	2.275e-05	0.0000
0.4	p_offset	0.0040766	0.0041405	0.0000
0.8	stack_io	0.033128	0.033135	0.0000
0.8	stack_alpha	0.30106	0.30099	0.0000
0.8	stack_t_membrane	-0.24759	-0.24744	0.0000
0.8	env_RH	0.00058119	0.00028542	0.0000
0.8	p_offset	-0.0587	-0.058375	0.0000
1.16	stack_io	0.02497	0.024953	0.0000
1.16	stack_alpha	0.26278	0.17482	0.0000
1.16	stack_t_membrane	-0.22414	-0.13618	0.0000
1.16	env_RH	0.00059453	0.00029286	0.0000
1.16	p_offset	-0.061831	-0.061789	0.0000

The normalized local sensitivity coefficients were computed using a central difference scheme with ±10% perturbations around each baseline parameter value. Results are reported at $j_{\text{low}} = 0.4\,\text{A/cm}^2, j_{\text{mid}} = 0.8\,\text{A/cm}^2$ and $j_{\text{high}} = 1.16\,\text{A/cm}^2$. The parameters *stack_io*, *stack_alpha*, and *stack_t_membrane* capture activation and ohmic loss drivers in the MEA model, while *env_RH* and *p_offset* represent boundary and control conditions that affect hydration and operating pressure. The results show that voltage and net power sensitivities increase with load for the dominant electrochemical parameters. In contrast, *S_H2* is approximately zero for all tested parameters because, at fixed commanded current density, hydrogen consumption over each window is constrained primarily by Faraday's law and is weakly influenced by these parameter perturbations.

C. *Consistency checks over a 2500 s dynamic power-demand profile*

Over the custom 2500 s power-demand profile, the model produces time-dependent values of stack power, auxiliary power, net delivered power, and stack heat dissipation, as shown in Fig. 7. The imposed demand ranges from 0 to 95.8 kW, with a mean value of 22.8 kW, and includes repeated low-, medium-, and high-load excursions. The power balance shows that auxiliary loads increase during high-load intervals, where the air compressor becomes the dominant consumer and reduces usable net power. The heat dissipation trace follows the load level and increases during high-power excursions, confirming the expected coupling between electrical production, losses, and thermal management demand. The same trends observed in quasi-steady operation also appear under dynamic excitation.

As a qualitative consistency check, the model response was compared with expected PEMFC behavior reported in the literature, including decreasing cell voltage with increasing current density, decreasing LHV efficiency at higher load, and increasing compressor demand with air-flow requirement. A full experimental validation against measured stack data remains future work.

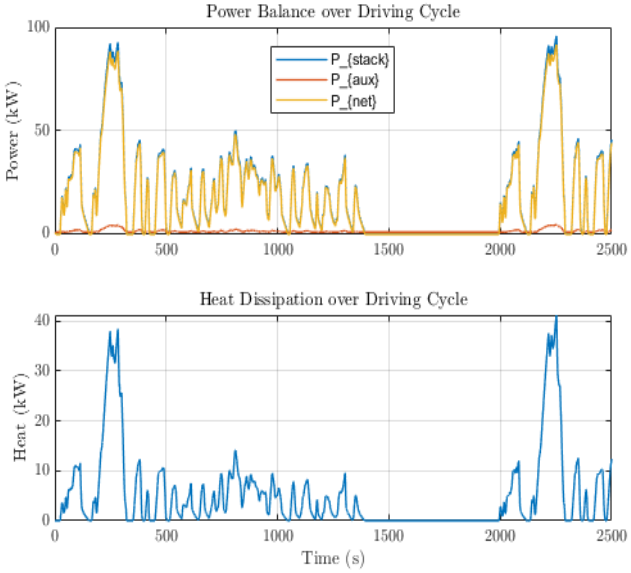

Fig. 7. Power balance and heat dissipation over the custom 2500 s dynamic power-demand profile: stack power, auxiliary power, and net power (top), and stack heat dissipation (bottom).

IV. CONCLUSIONS

This paper presented a reproducible system-level evaluation workflow for an automotive PEM fuel cell system model using LHV-referenced energy metrics. Quasi-steady operating points extracted from a stepped power profile yielded consistent polarization behavior and coherent trends in net power, efficiency, and reactant utilization, while explicitly quantifying auxiliary power penalties. A normalized local sensitivity analysis at three load levels ranked the parameters that most strongly affect V_{cell} and P_{net}, enabling targeted calibration and uncertainty reduction. The same

analysis indicated near-zero sensitivity of integrated hydrogen consumption to the selected parameter set under fixed commanded current density, consistent with Faraday-limited fuel use over each window. A custom 2500 s dynamic power-demand profile confirmed that the quasi-steady trends persist under dynamic operation and showed that compressor demand becomes the dominant contributor to net power reduction at higher loads. Future work will extend the model with explicit anode hydrogen inventory, purge dynamics, auxiliary efficiency maps, advanced thermal management, compressor operating-point optimization, degradation-aware PEMFC modeling, and possibly AI-based supervisory control strategies for dynamic load operation.

APPENDIX

The following nomenclature was used in this paper:

j – current density, A/cm²
I_{stack} – stack current, A
$t, t_1, t_2 -$ $t$ime and averaging-window bounds, s
T_{avg} – averaging window length, s
V_{cell} – cell voltage, V
V_{stack} – stack voltage, V
P_{stack} – stack electrical power, kW
P_{comp} – compressor power, kW
P_{pump} – coolant pump power, kW
P_{aux} – auxiliary power, kW
P_{net} – net power delivered, kW
η_{LHV} – efficiency based on hydrogen LHV, %
LHV_{H2} – hydrogen lower heating value, kWh/kg
E_{spec} – specific electrical energy per hydrogen mass, kWh/kg
E_{el} – electrical energy produced over an interval, kWh
$S_{y,\theta}$ – normalized local sensitivity
$m_{\text{H2},cons}$– consumed hydrogen mass, kg
$\dot{m}_{\text{H2,in}}$ – hydrogen inlet mass flow rate, kg/s
$\dot{m}_{\text{H2,out}}$ – hydrogen outlet mass flow rate, kg/s
$\dot{m}_{\text{O2}}$ – oxygen mass flow rate, kg/s
U_{H2} – hydrogen utilization factor, pu
$p_{\text{an,in}}$ – anode inlet pressure, bar
$p_{\text{ca,in}}$ – cathode inlet pressure, bar
rpm_{comp} – compressor speed, rpm
T_{set} – stack temperature setpoint, °C
r_{H} – relative humidity setpoint, pu
stack_io – exchange current density parameter (MEA), model parameter
stack_alpha - charge transfer coefficient parameter (MEA), model parameter
stack_t_membrane – membrane thickness, μm
env_RH – ambient or boundary relative humidity parameter, pu
p_offset – pressure-control offset parameter, model parameter
S_V – normalized sensitivity of V_{cell}
S_P – normalized sensitivity of P_{net}
S_{H2} – normalized sensitivity of hydrogen consumption

REFERENCES

[1] E. D. Maer, D. Fodorean, and A. A. Șpaimoc, "The Evolution of Fuel Cells: State-of-the-Art and Emerging Trends," in Proc. 2025 Int. Conf. on Electromechanical and Energy Systems (SIELMEN), 2025, pp. 426–431, doi: 10.1109/SIELMEN67352.2025.11260676.

[2] J. T. Pukrushpan, A. G. Stefanopoulou, and H. Peng, Control of Fuel Cell Power Systems: Principles, Modeling, Analysis and Feedback Design, 2004.

[3] J. Larminie and A. Dicks, Fuel Cell Systems Explained, 2nd ed., Wiley, 2003.

[4] R. O'Hayre, S.-W. Cha, W. Colella, and F. B. Prinz, Fuel Cell Fundamentals, 3rd ed., Wiley, 2016.

[5] MathWorks, "PEM Fuel Cell System (Simscape)," online documentation.

[6] J. C. Amphlett et al., "A model predicting transient responses of proton exchange membrane fuel cells," Journal of Power Sources, 1995.

[7] T. E. Springer, T. A. Zawodzinski, and S. Gottesfeld, "Polymer electrolyte fuel cell model," Journal of The Electrochemical Society, 1991.

[8] A.-A. Șpaimoc, E.-D. Maer, and D. Fodorean, "Design and Modelling of a 100 kW Fuel Cell for EV Propulsion," in Proc. 2025 Int. Conf. on Electromechanical and Energy Systems (SIELMEN), 2025, pp. 436–441, doi: 10.1109/SIELMEN67352.2025.11260672.

[9] C. Acar and I. Dincer, "Hydrogen Production," in Comprehensive Energy Systems, vol. 3, 2018, pp. 1–40, doi: 10.1016/B978-0-12-809597-3.00304-7.

[10] G. M. Cabello González, B. Toharias, F. Rosa, J. J. Guerra, and A. Iranzo, "Temperature and Current Density distributions in a 100 cm2 PEM Fuel Cell: Effects of flow field designs," J. Power Sources, vol. 652, Oct. 1, 2025, Art. no. 237625.

[11] Y. Liu, J. Liu, and D. Q. Guang, "Online energy management strategy of fuel cell hybrid electric vehicles based on rule learning," J. Cleaner Prod., vol. 260, Jul. 2020, Art. no. 121017, doi: 10.1016/j.jclepro.2020.121017.

[12] L. Xu, J. Li, J. Hua, and X. Li, "Adaptive supervisory control strategy of a fuel cell/battery-powered city bus," J. Power Sources, vol. 194, no. 1, pp. 360–368, Oct. 2009, doi: 10.1016/j.jpowsour.2009.04.074.

[13] D. Fodorean, "High-Speed Electric Motors for Fuel Cell Compressor System Used for EV Application —Review and Perspectives", *Applied Sciences, vol.16*, nr.476, January, 2026.
https://doi.org/10.3390/app16010476.

[14] Z. Ding, H. Zhu, Z. Bai, and W. Zhou, "Research on Heat and Mass Transfer of Hydrogen Production from Green Electricity," in Proc. 2024 Int. Conf. on Electrical Drives, Power Electronics & Engineering (EDPEE), 2024, pp. 1031–1035,
doi: 10.1109/EDPEE61724.2024.00197.